

# Structural relaxation, dynamical arrest and aging in soft-sphere liquids

P. Mendoza-Méndez<sup>1</sup>, Ricardo Peredo-Ortiz<sup>1,2</sup>, Edilio Lázaro Lázaro<sup>1,2</sup>, M. Chávez-Paez<sup>2</sup>,  
H. Ruiz-Estrada<sup>1</sup>, F. Pacheco-Vázquez<sup>3</sup>, M. Medina-Noyola<sup>2</sup> and L.F. Elizondo-Aguilera<sup>3\*</sup>

<sup>1</sup> *Facultad de Ciencias Físico-Matemáticas,*

*Benemérita Universidad Autónoma de Puebla,*

*Apartado Postal 1152, CP 72000, Puebla, PUE, México*

<sup>2</sup> *Instituto de Física, Universidad Autónoma de San Luis Potosí,*

*Álvaro Obregón 64, 78000 San Luis Potosí, SLP, México and*

<sup>3</sup> *Instituto de Física, Benemérita Universidad Autónoma de Puebla,*

*Apartado Postal J-48 72520, Puebla, México\**

(Dated: August 18, 2022)

## Abstract

We investigate the structural relaxation of a soft-sphere liquid quenched isochorically ( $\phi = 0.7$ ) and instantaneously to different temperatures  $T_f$  above and below the glass transition. For this, we combine extensive Brownian dynamics simulations and theoretical calculations based on the non-equilibrium self-consistent generalized Langevin equation (NE-SCGLE) theory. The response of the liquid to a quench generally consists of a sub-linear increase of the  $\alpha$ -relaxation time with system's age. Approaching the ideal glass-transition temperature from above ( $T_f > T^a$ ) sub-aging appears as a transient process describing a broad equilibration crossover for quenches to nearly arrested states. This allows us to empirically determine an equilibration timescale  $t^{eq}(T_f)$  that becomes increasingly longer as  $T_f$  approaches  $T^a$ . For quenches inside the glass ( $T_f \leq T^a$ ) the growth rate of the structural relaxation time becomes progressively larger as  $T_f$  decreases and, unlike the equilibration scenario,  $\tau_\alpha$  remains evolving within the whole observation time-window. These features are consistently found in theory and simulations with remarkable semi-quantitative agreement, and coincide with those revealed in the similar and complementary exercise [Phys. Rev. **96**, 022608 (2017)] that considered a sequence of quenches with fixed final temperature  $T_f = 0$  but increasing  $\phi$  towards the hard-sphere dynamical arrest volume fraction  $\phi_{HS}^a = 0.582$ . The NE-SCGLE analysis, however, unveils various fundamental aspects of the glass transition, involving the abrupt passage from the ordinary equilibration scenario to the persistent aging effects that are characteristic of glass-forming liquids. The theory also explains that, within the time window of any experimental observation, this can only be observed as a continuous crossover.

PACS numbers: 23.23.+x, 56.65.Dy

---

\* luisfer.elizondo@gmail.com

## I. INTRODUCTION.

Aging is a fundamental aspect of the process of amorphous solidification observed in glass and gel-forming liquids upon undercooling [1–7]. It is embodied in a slow and long-lasting evolution of the physical observables with the waiting time  $t$  after preparation, and it is consistently found in a wide variety of microscopically very different materials, ranging from polymers [8, 9], metallic alloys [10, 11], aqueous clay suspensions [12–14] and colloids [15–20], thus revealing its universal character.

In contrast with the number of experimental [21–24] and computer simulation [25–28] investigations carried out to quantify the irreversible relaxation in a variety of model systems during aging, only a few first-principles theoretical approaches [29, 30] are available for the description and understanding of such out-of-equilibrium processes. In particular, about two decades ago Latz [31–33] formally extended the well established mode coupling theory (MCT) of the glass transition (GT) [34–37] to allow for the description of aging. However, no quantitative predictions have been presented so far that could be contrasted with experimental or simulation results for specific model systems of structural glass-formers. Thus, one can state that until recently, no quantitative first-principles theory has been developed and applied to successfully describe aging phenomena in structural glass-forming (atomic or colloidal) liquids.

In this regard, similar developments to those made by Latz were carried out in the context of the so-called self-consistent generalized Langevin equation (SCGLE) theory of colloid dynamics [38–42] and dynamical arrest [43–45]. In this manner, this theory, which can be regarded as an alternative to MCT [46], could be extended to non-equilibrium conditions, allowing the description of the spatially non-uniform and temporally non-stationary relaxation of glass-forming liquids. Such an extension, carried out in Ref. [47] and referred to as the *non-equilibrium* self-consistent generalized Langevin equation (NE-SCGLE) theory, led to the emergence of a quantitative first-principles description of aging in structural glass formers.

The theoretical framework provided by the NE-SCGLE has solidly demonstrated its ability to predict some of the most relevant universal signatures of both, the glass and gel transitions, including aging effects, as well as very specific features reflecting the particular role of molecular interactions in the explicit systems considered. For example, this theory ac-

curately describes the process of formation of high-density hard-sphere-like glasses [48–51], whereas for low-density and low-temperature liquids with excluded volume plus attractive interactions it predicts the formation of sponge-like gels and porous glasses by arrested spinodal decomposition [52–55]. The comparison of such predictions with both, experimental and simulated data for systems with essentially the same kind of molecular interactions, confirms that the NE-SCGLE is a successful non-equilibrium statistical mechanics approach for the description of the slowing down and the aging of the dynamics observed in glass- and gel-forming liquids.

Let us refer, in particular, to the scenario predicted by this theory when the Weeks-Chandler-Andersen (WCA) soft-sphere liquid is suddenly and isochorically quenched to zero temperature within the constraint that it remains spatially uniform. This scenario was first systematically analyzed using the NE-SCGLE theory in Ref. [49]. Such study considers a series of independent quench processes that differ only in the value of the fixed density  $n$ . Each of these processes starts with the repulsive liquid in an equilibrium (fluid-like) state of density  $n$  and initial temperature  $T_i$ . Afterwards, the system is instantaneously quenched to a final temperature value  $T_f = 0$ . Since the zero-temperature limit of such soft-sphere fluid is actually a hard-sphere (HS) liquid of volume fraction  $\phi$ , these processes mimic the spontaneous search for the equilibrium state of a HS liquid, driven to non-equilibrium conditions by some perturbation (shear, for example [56, 57]) that ceases at a time  $t = 0$ .

For each of these isochoric processes, the NE-SCGLE described the irreversible relaxation of the system in terms of the time-evolution of the *non-equilibrium* structure factor (SF)  $S(k; t)$  and of dynamical properties, such as the *self* intermediate scattering function (ISF)  $F_S(k, \tau; t)$ , where  $\tau$  is the correlation (or *delay*) time and  $t$  is the waiting (or *evolution*) time after the quench. In particular, the predicted  $t$ -development of the  $\alpha$ -relaxation time  $\tau_\alpha(t)$  (with  $F_S(k, \tau_\alpha; t) = 1/e$ ) allowed for the identification of an *equilibration time*  $t^{eq}(\phi)$ , defined as the time-scale after which  $\tau_\alpha(t)$  saturates to its equilibrium value  $\tau_\alpha^{eq}(\phi)$ . Thus, according to the NE-SCGLE one possibility is that the quenched hard-sphere liquid will recover equilibrium within a finite time window  $t^{eq}(\phi)$  that depends on the specific value of the (fixed) volume fraction  $\phi$ . However, both  $t^{eq}(\phi)$  and  $\tau_\alpha^{eq}(\phi)$  are also predicted to diverge as  $\phi$  approaches the HS dynamical-arrest volume fraction  $\phi_{HS}^a$  from below. Let us recall that, according to the *equilibrium* SCGLE theory [50], the HS system remains ergodic for  $0 < \phi < \phi_{HS}^a = 0.582$  and becomes dynamically arrested at  $\phi = \phi_{HS}^a$  and beyond. Hence,

for quenches with  $\phi \geq \phi_{HS}^a$ , the prediction is that the system will no longer be able to equilibrate, but instead, will age forever during the endless process of becoming a glass.

Furthermore, another relevant prediction of the NE-SCGLE theory for the quench processes considered is that, for a fixed *finite* waiting time  $t$ , the plot of  $\tau_\alpha(t; \phi)$  as a function of  $\phi$  exhibits two regimes, corresponding to samples that have fully equilibrated within this waiting time ( $\phi \leq \phi_0(t)$ ), and to samples for which equilibration is not yet complete ( $\phi \geq \phi_0(t)$ ). The crossover volume fraction  $\phi_0(t)$  increases with  $t$  but saturates to the value  $\phi_{HS}^a$ . These predictions have been contrasted against analogous results of extensive molecular dynamics simulations finding a remarkable consistency [50, 51].

The work in Refs. [49–51], however, leaves open several important issues. One of them refers to the fact that the physical scenario just described is conceptually closer to the spontaneous equilibration or aging of a non-equilibrium HS colloidal dispersion [56, 57], in which the volume fraction  $\phi$  is the relevant control parameter. However, in other aging experiments involving actual soft-sphere colloidal suspensions (made of, *e.g.*, thermosensitive microgel colloids [58, 59]) it is temperature (and/or softness) rather than volume fraction, the relevant control parameter. Such colloidal quench experiments are, in fact, conceptually closer to the equilibration and aging of atomic glass-formers [5]. Experience indicates that in thermally-driven systems the inverse temperature  $T^{-1}$  plays a qualitatively analogous role to that of the volume fraction  $\phi$  in density-driven colloidal systems. Thus, an obvious question is whether the NE-SCGLE theory has the ability to explain in more precise terms this conceptually important empirical analogy. Addressing this well-defined challenge constitutes the main objective of the present contribution.

With this objective in mind, we have carried out extensive Brownian dynamics simulations, as well as theoretical calculations within the NE-SCGLE framework, which we combine to study the irreversible relaxation and the GT in the same soft-sphere system as in Refs. [49–51]. As just mentioned, these references involved a sequence of isochoric quenches to the same final temperature  $T_f = 0$ , but along different isochores (*i.e.*, different volume fractions  $\phi$ ). In contrast, in this work we investigate the complementary study, involving a sequence of isochoric quenches, now along a given isochore with fixed volume fraction  $\phi (> \phi_{HS}^a = 0.582)$ , but with different final  $T_f$ , both above and below the dynamical arrest line  $T = T^a(\phi)$  (solid curve in Fig. 1 below). We then analyze the concomitant relaxation of the system in terms of the waiting-time evolution of the structural and dynamical properties provided by both,

simulations and theory, as a function of the control parameter  $T_f$ .

As in Ref. [47], here we find two qualitatively different scenarios for the relaxation of the dynamics, identified through the specific evolution of the  $\alpha$ -relaxation time  $\tau_\alpha(t)$  after quenching. The first involves quenches with  $T_f > T^a(\phi)$ , for which  $\tau_\alpha(t)$  shows a transient increase with system's age before attaining a new stationary equilibrium value  $\tau_\alpha^{eq}(T_f)$ . This behavior, in turn, allows us to obtain an empirical relation for the equilibration time  $t^{eq}(T_f)$  of the system, which grows as a power law of  $\tau_\alpha^{eq}(T_f)$  with exponent larger than one. A second scenario is found for quenches with  $T_f \leq T_a(\phi)$ , in which we observe that  $\tau_\alpha(t)$  grows sub-linearly with waiting time and, unlike the equilibration scenario, the structural relaxation time exhibits a persistent development over the entire observation time-window, showing also an increasingly larger growth rate as  $T_f$  becomes smaller. All these features are consistently observed in simulations and theory, finding only small deviations at the longest waiting times explored.

The main results of this contribution are conveniently summarized in a plot of  $\tau_\alpha(t; 1/T)$  vs  $1/T$ , thus allowing us to compare the overall physical scenario obtained here with that previously reported in Refs. [50, 51], corresponding to the hard-sphere limit ( $T_f = 0$ ) of the same glass-forming liquid. Such a comparison elucidates the qualitative correspondence of the two control parameters  $\phi$  and  $1/T$  in determining the non-equilibrium relaxation of a soft-sphere liquid quenched towards the GT.

Our work is organized as follows: In section II we briefly describe the model soft-sphere liquid studied with simulations and theory. To serve as a reference, in the same section we also present the arrested states diagram predicted by the NE-SCGLE for such system, along with the sequence of quenches employed to investigate its irreversible relaxation. In section III we focus on the description of the process of equilibration at the level of both structural and dynamical properties, with the former allowing us to determine the aforementioned equilibration time-scale of the system. Section IV addresses the description of the crossover from equilibration to the dynamical arrest and aging regime. For clarity and methodological convenience, this section is divided in three parts. In subsection IV A we present and discuss the main results of our BD simulations for the kinetic evolution of the system for quenches below the critical temperature  $T^a$ . In subsections IV B and IV C, respectively, the non-equilibrium relaxation of the structural and dynamical properties during the development of glassy states is explained and discussed within the theoretical framework provided by

the NE-SCGLE. In section [V](#) we describe the connection between our results and previous findings for the HS limit of the same model system considered here, thus allowing to establish the qualitative correspondence of the two control parameters  $\phi$  and  $T$  in determining the non-equilibrium relaxation of the quenched soft-sphere fluid. Finally, in Sec. [VI](#) we summarize our main conclusions. For clarity, a brief review of the NE-SCGLE equations is provided in appendix [A](#), whereas the main details of our BD simulations are described in appendix [B](#).

## II. TEMPERATURE-QUENCHED SOFT-SPHERE SYSTEM: DYNAMICAL ARREST DIAGRAM

In in this work we will study the structural relaxation of a monocomponent Brownian fluid constituted by  $N$  soft-spheres of diameter  $\sigma$  in a volume  $V$ , interacting through a Weeks-Chandler-Anderson (WCA) potential [\[60\]](#), that vanishes for  $r$  larger than the distance  $\sigma$  of soft contact, but which for  $r \leq \sigma$  is given by

$$u(r) = \epsilon \left[ \left( \frac{\sigma}{r} \right)^{12} - 2 \left( \frac{\sigma}{r} \right)^6 + 1 \right]. \quad (2.1)$$

The state space of this model system is spanned by the volume fraction  $\phi = \pi n \sigma^3 / 6$  (with  $n = N/V$ ) and the effective temperature  $T^* \equiv k_B T / \epsilon$ . For simplicity, from now on we shall refer to the dimensionless parameter  $T^*$  just as  $T$  and use  $\sigma$  and  $[\sigma^2 / D^0]$  as the units of length and time, respectively, with  $D^0$  being the short-time self-diffusion coefficient, related to the corresponding short-time friction coefficient  $\zeta^0$  by Einstein's relation  $\zeta^0 = k_B T / D^0$ . For colloidal liquids  $\zeta^0$  can be determined by its conventional Stokes expression, whereas for atomic liquids  $\zeta^0$  represents the less intuitive Doppler friction [\[61, 62\]](#).

To organize our discussion, let us start by considering [Fig. 1](#), which displays the dynamical arrest diagram predicted by the NE-SCGLE theory for the WCA fluid just described. Except for trivial modifications explained below, this figure is [Fig. 1](#) of Ref. [\[49\]](#). The same reference provides all the pertinent numerical details. This diagram identifies two different regions of the  $(\phi, T)$ -plane, corresponding to asymptotically stationary ergodic (fluid) and non-ergodic (dynamically arrested) states. The boundary between these regions is delimited by the ideal isodiffusivity line  $D^L(\phi, T) = 0$ , with  $D^L$  being the long-time diffusion coefficient. This condition defines a dynamical arrest temperature  $T^a(\phi)$  which, for  $\phi > \phi_{HS}^a$ , describes a monotonically increasing function of the packing fraction (solid curve in [Fig. 1](#)).

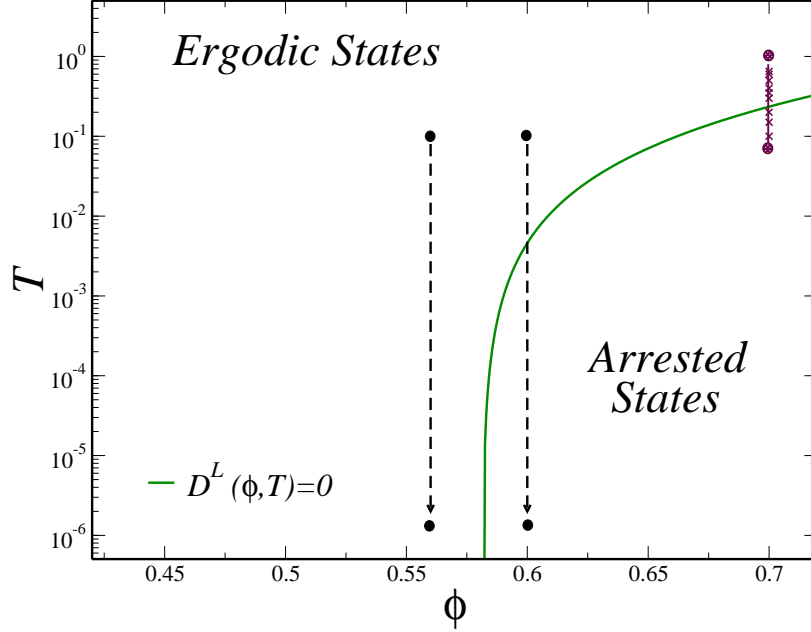


FIG. 1. Dynamical arrest diagram of the WCA model defined in Eq. (2.1), predicted by the NE-SCGLE using the numerical solution of the Ornstein-Zernike equation and the Percus-Yevick/Verlet-Weis approximation [63, 64] for the determination of the thermodynamical inputs required by the theory (see Sec. IIIA of Ref. [49]). The solid line that separates the regions of ergodic and arrested states corresponds to the locus of the ideal isodiffusivity line  $D^L(\phi, T) = 0$ . The dashed vertical arrows on the left represent the two qualitatively distinct types of quench processes studied in Ref [49], corresponding to isochoric quenches at fixed  $\phi = 0.56 < \phi_{HS}^a$  and  $\phi = 0.6 > \phi_{HS}^a$ , from an initial temperature  $T_i = 0.1$  and with final value  $T_f = 0$ , thus describing the processes of equilibration and aging in a HS fluid, respectively. The solid arrow in the top right represents, instead, a sequence of isochoric quenches at fixed  $\phi = 0.7$ , all of which start from the same initial temperature  $T_i = 1$ , but end at different values of  $T_f$ , used here to describe the crossover from equilibration,  $T_f > T^a(\phi = 0.7)$ , to aging,  $T_f \leq T^a(\phi = 0.7)$ , with  $T^a(\phi = 0.7) = 0.235$ .

As we show in what follows, for any isochoric quench from the ergodic region (with  $\phi > \phi_{HS}^a$ ) the critical value  $T^a(\phi)$  separates two possible and mutually exclusive regimes for the relaxation of the dynamics of the WCA system, corresponding to equilibration (for quenches with  $T_f > T^a(\phi)$ ) or dynamical arrest and aging (for  $T_f \leq T^a(\phi)$ ), with  $T^a(\phi = 0.7) = 0.235$ .

As already mentioned, these two scenarios were analyzed in detail in Ref. [49], but only



for the specific case in which the system defined in Eq.(2.1) is instantaneously quenched from the ergodic region to a final temperature  $T_f = 0$ . As emphasized in the introduction, in this work we are interested in the study of the complementary category of thermally-driven processes that consider, instead, quenches to a finite value  $T_f \neq 0$ . Thus, in what follows we analyze a sequence of isochoric quenches ( $\phi = 0.7$ ), all of which start from the same state point in the high density/high temperature ergodic regime and whose final temperature  $T_f$  gradually approaches and crosses the critical value  $T^a(\phi = 0.7)$ . These processes are illustrated by the solid arrow and cross symbols in the top right of Fig.1.

### III. EQUILIBRATION OF THE WCA MODEL AFTER A QUENCH.

For clarity and methodological convenience, we will first discuss the conceptually simplest scenario for the relaxation of the WCA liquid. We refer to the process of full equilibration, corresponding to the case in which this system, originally at equilibrium, is quenched to a final state that also lies in the ergodic region (*i.e.*,  $T_f > T^a(\phi)$ ). As discussed in Refs. [47–50], the relaxation of the quenched liquid can be described in terms of the time-evolution of the non-equilibrium SF,  $S(k; t) \equiv \langle \delta n(\mathbf{k}; t) \delta n^\dagger(-\mathbf{k}; t) \rangle$ , with  $\delta n(\mathbf{k}; t)$  being the Fourier transform of the fluctuations in the number density  $n(\mathbf{r}; t) = \sum_{i=1}^N \delta(\mathbf{r} - \mathbf{r}_i(t)) / \sqrt{N}$ , and also in terms of the *self* intermediate scattering function (ISF)  $F_S(k; \tau; t) = \langle \exp[i\mathbf{k} \cdot \Delta \mathbf{r}_T(\tau, t)] \rangle$ , with  $\Delta \mathbf{r}_T(\tau, t) \equiv [\mathbf{r}_T(t + \tau) - \mathbf{r}_T(t)]$  being the displacement of a tracer particle and where the angular brackets indicate average over a time-dependent non-equilibrium statistical ensemble. In what follows, we will stick to the analysis of these two properties. For reference, a brief summary of the NE-SCGLE equations describing the  $t$ -evolution of these quantities is provided in Appendix A. The details of our BD simulations are provided in Appendix B.

Before discussing our results, let us recall that solving the NE-SCGLE equations (Eqs. (A1)-(A6) of Appendix A) requires the previous determination of the fundamental thermodynamic input  $\mathcal{E}(k; n, T)$  involved in Eq. (A1), related to the FT of the two-particle direct correlation function  $c[|\mathbf{r} - \mathbf{r}'|; n; T]$ , and to the equilibrium structure factor  $S^{eq}(k; n, T)$  by  $n\mathcal{E}(k; n, T) = 1 - nc(k; n, T) = 1/S^{eq}(k; n, T)$ . As explained in detail in Ref. [49], in our present case this property can be determined using the Ornstein-Zernike (OZ) equation combined with the Percus-Yevick/Verlet-Weiss (PY-VW) approximation [63, 64] for an effective HS fluid with a  $T$ -dependent HS diameter  $\sigma(T)$  obtained by the blip function method

[65] (see also Sec. IIIA of Ref. [49]). The demonstrative diagram of Fig. 1 was in fact calculated in this manner, leading to the value  $T^a(\phi = 0.7) = 0.235$  of the dynamic arrest temperature along the isochore  $\phi = 0.7$  quoted above. In what follows, however, we shall introduce a slight modification of this procedure to fine-tune the quantitative comparison between theory and simulations.

Thus, to analyze relaxation processes corresponding to comparable initial and final states, we have fine-tuned the previous approximate determination of the thermodynamic input, which we denote as  $\mathcal{E}_{PY/VW}(k; n, T)$ . For this we used well-equilibrated simulation results for the static structure factor  $S_{BD}^{eq}(k; \phi = 0.7, T)$  at a set of values of the temperature  $T$ , to determine a rescaled theoretical temperature  $T'(T)$  such that the height of the main peak of the theoretical structure factor  $S_{PY/VW}^{eq}(k; \phi = 0.7, T') \equiv 1/n\mathcal{E}_{PY/VW}(k; \phi = 0.7, T')$  fits the height of the main peak of  $S_{BD}^{eq}(k; \phi = 0.7, T)$ . This procedure leads to the approximate rescaled temperature  $T' = (3.2)T^{0.785}$ . In addition, following previous work [50, 51] we have also employed the simulation values of the equilibrium mobility  $b^{eq}(\phi = 0.7, T)$  to calibrate the only free parameter of the NE-SCGLE, namely, the cutoff wave-vector  $k_c$  (see Eq. (A6)), leading to the choice  $k_c = 2.05 \times 2\pi/\sigma$ . The changes resulting from the previous rescaling of  $T$  and calibration of  $k_c$  are only quantitative. For example, the new value of the dynamic arrest temperature along the isochore  $\phi = 0.7$  is  $T^a(\phi = 0.7) = 0.166$  (compared to the previous value  $T^a(\phi = 0.7) = 0.235$  quoted above).

Fig. 2 summarizes the results obtained with both, simulations (upper panels) and theory (lower panels), for the description of the process of equilibration of the WCA fluid after an instantaneous isochoric quench from the initial state point ( $\phi = 0.7, T_i = 1.0$ ) to a final temperature  $T_f = 0.25$ . Figs. 2(a) and 2(d), for instance, display a sequence of snapshots at waiting times  $t = 0, 10^{-3}, 10^{-2}, 10^{-1}, 10^0, 10^1$  and  $10^2$  describing the evolution of the SF after quenching. At  $t = 0$  (open symbols in both figures) the function  $S_i(k)$  shows the typical behavior of a dense repulsive liquid, mainly characterized by the development of a well defined peak at  $k = k_{max} \approx 7.7$ , and oscillations around the unitary value for larger wave-vectors. After the quench ( $t > 0$ ), the SF gradually evolves describing an ordinary de Gennes narrowing [66], which consists of a notorious amplification of the structural correlations around  $k_{max}$  (see the inset of both figures) and also a small shift of the second peak towards slightly smaller  $k$  values. At a time-scale of order  $10^1$ ,  $S(k, t)$  ceases to evolve and reaches a new (equilibrium) stationary value  $S_f(k)$  (solid symbols). All these features, which describe

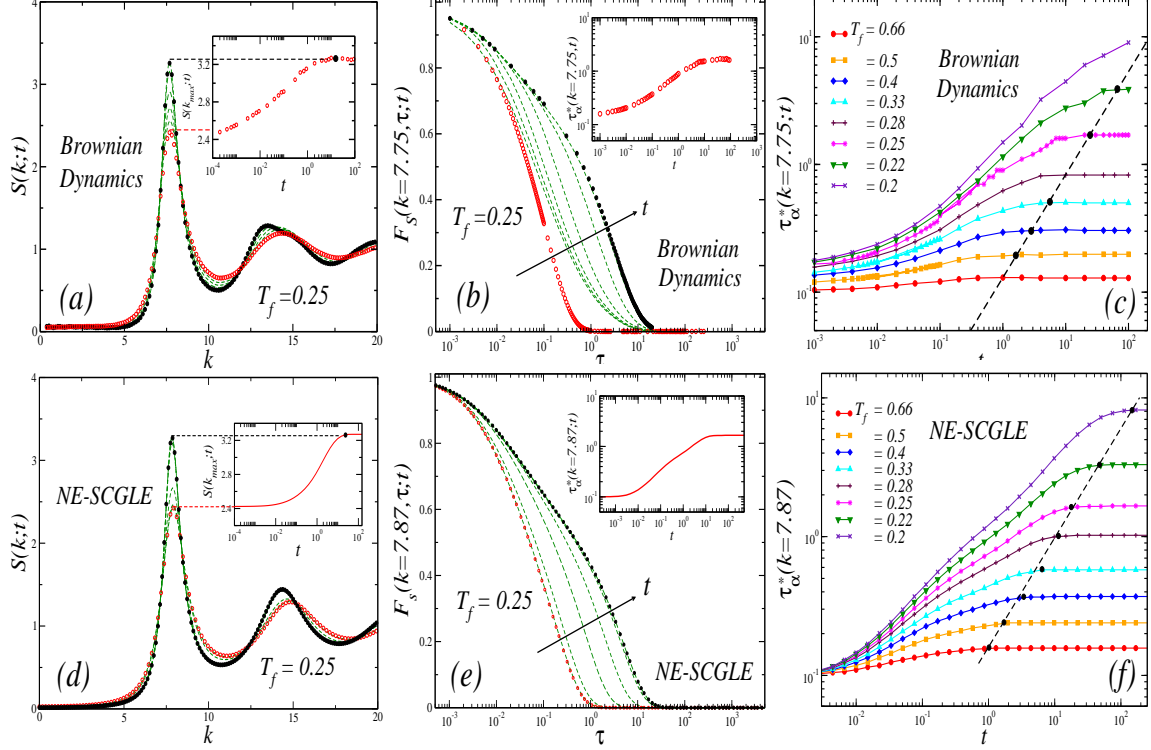


FIG. 2. Schematic representation of an equilibration process of the WCA fluid after an instantaneous isochoric quench from the equilibrium state point ( $\phi = 0.7, T_i = 1$ ) to a final temperature  $T_f$  above the dynamical arrest point  $T^a = 0.166$ . (a) and (d) Sequence of snapshots at waiting times  $t = 10^{-3}, 10^{-2}, 10^{-1}, 10^0, 10^1$  and  $10^2$  (green dashed lines) obtained from BD simulations and theory, respectively, describing the waiting time evolution of the SF  $S(k, t)$  from its initial value,  $S_i(k) = S(k; t = 0) = S^{eq}(k; \phi = 0.7, T_i = 1)$  (open symbols), towards a final equilibrium value  $S_f(k) = S^{eq}(k; \phi = 0.7, T_f = 0.25)$  (solid symbols). In both figures, the inset emphasizes the time-evolution of the maximum  $S_{max}(t) \equiv S(k = k_{max}; t)$  of the SF. (b) and (e) Corresponding sequence of snapshots for the self-ISF  $F(k, t)$ . In both figures, the inset highlights the evolution of the  $\alpha$ -relaxation time  $\tau_\alpha(t)$ , scaled as  $\tau_\alpha^*(t) \equiv k_{max}^2 D^0 \tau_\alpha(t)$ , for the specific quench considered. (c) and (f) Waiting time dependence of  $\tau_\alpha^*(t)$  for a sequence of quenches at various  $T_f$  above and approaching the transition temperature  $T^a(\phi = 0.7)$ . The dark circles along the dashed lines in both figures illustrate the relationship between the equilibration time  $t^{eq}(\phi = 0.7, T_f)$  and the equilibrium  $\alpha$ -relaxation time  $\tau_\alpha^{eq}(\phi = 0.7, T_f)$  of each quench (see text).

the typical structural behavior of a soft-sphere fluid upon cooling, are consistently found in both, simulations and theory.

As shown in Figs. 2(b) and 2(e), for this kinetic process one also finds a gradual slowing down in the dynamics. This is observed in the increasingly slower  $\tau$ -relaxation displayed by the ISF  $F_S(k, \tau; t)$  as  $t$  becomes larger or, equivalently, in the development of the  $\alpha$ -relaxation time  $\tau_\alpha(k; t)$  (defined by the condition  $F_S(k, \tau_\alpha; t) = 1/e$ ) with waiting-time. One notices, for instance, that  $\tau_\alpha(t)$  grows roughly one order of magnitude during the time-scale of evolution of the SF (see the insets of Figs. 2(b) and 2(e)). For larger  $t$ , the ISF stops evolving and reaches a new stationary value  $F_S^{eq}(k; \tau)$  (solid symbols), so that the  $\alpha$ -relaxation time saturates to a constant  $\tau_\alpha^{eq}(T_f)$ , thus indicating the full equilibration of the system.

In order to emphasize the role of the final temperature of a quench on the slowing down and equilibration of the dynamics, we might consider the behavior of  $\tau_\alpha(t)$  for a sequence of quenches with decreasing  $T_f$ . This is done in Figs. 2(c) and 2(f), which show the results obtained with simulations and theory, respectively, for the evolution of the  $\alpha$ -relaxation time, scaled as  $\tau_\alpha^*(t) \equiv k_{max}^2 D^0 \tau_\alpha(t)$  and for different values of  $T_f$ , as indicated. Thus presented, these results highlight the transient increase in the  $\alpha$ -relaxation time during times shorter than the  $T_f$ -dependent equilibration time  $t^{eq}(T_f)$ , after which  $\tau_\alpha(t)$  has saturated at its corresponding equilibrium value  $\tau_\alpha^{eq}(\phi = 0.7, T_f)$ . Notice that both,  $\tau_\alpha^{eq}(\phi = 0.7, T_f)$  and  $t^{eq}(T_f)$  become increasingly larger with decreasing  $T_f$ . For reference, the equilibration times found in simulations and theory are represented in Figs. 2(c) and 2(f) by the solid black circles. One notices that these highlighted values align themselves to a good approximation along the dashed straight lines, which thus define an empirical relationship of the form

$$\tau_\alpha^{eq}(T_f) \approx A \times [t^{eq}(T_f)]^\gamma, \quad (3.1)$$

that can also be written as  $t^{eq}(T_f) \propto [\tau_\alpha^{eq}(T_f)]^\eta$ , with  $\eta = 1/\gamma$ . From the Brownian dynamics simulation results in Fig. 2(c) we determine the values  $A_{BD} = 0.13$  and  $\gamma_{BD} = 0.8063$ , i.e.,  $t^{eq} \propto [\tau_\alpha^{eq}]^{1.24}$ . These values may be compared with those determined in Ref. [50] from the molecular dynamics simulation of a sequence of quenches that approach dynamic arrest by increasing the volume fraction:  $A_{MD} = 2.5$  and  $\gamma_{MD} = 0.7$ , which lead to  $t^{eq}(T_f) \propto [\tau_\alpha^{eq}(T_f)]^{1.43}$ . This means that these simulations (in agreement with others [67]) establish that as the glass transition is approached, i.e., as  $t^{eq}$  and  $\tau_\alpha^{eq}$  increase without bound, the former will always increase faster than the latter. Let us also highlight the fact that the apparent instantaneous slope  $\mu(t) \equiv [d \log \tau_\alpha(t) / d \log t]$  of the simulation results for  $\tau_\alpha(t)$  in Fig. 2(c) is always smaller than the slope of the dashed straight line of the figure, which

is itself smaller than unity. In other words, the simulated equilibration processes in Fig. 2(c) indicate that  $\mu(t) < 1$ . In addition, let us also notice that the simulation data for  $\log \tau_\alpha(t)$  as a function of  $\log t$  exhibits a point of inflection, below which  $\mu(t)$  increases with  $t$ , while above which it decreases. As  $T_f$  becomes smaller, however, this inflection point evolves into a finite and increasingly larger  $t$ -interval in which  $\mu(t)$  appears nearly constant, thus suggesting that  $\tau_\alpha(t)$  grows as a power law of the form  $\tau_\alpha(t) \propto t^\delta$  ( $\delta < 1$ ) within such interval. We will come back to this point later in Sec. IV D

In a first attempt to see if the NE-SCGLE theory captures these important conclusions, we first analyzed the data for  $\tau_\alpha(t)$  in Fig. 2(f) using the theoretical definition of the equilibration time  $t^{eq}$  given in Eq. (4.5) of Ref. [49]. As a result, we found that the theoretical predictions actually exhibited the opposite trend, namely, that  $t^{eq} \propto [\tau_\alpha^{eq}]^\eta$ , with the exponent  $\eta = 1/\gamma = 1/1.07 = 0.93$  being smaller, not greater, than one. Let us mention that this result is consistent with the NE-SCGLE result  $\eta = 1/\gamma = 1/1.05 = 0.95$  determined in Ref. [49] for the quench processes studied there. Hence, both predictions oppose the trends established by simulations. As it happens, however, such tentative NE-SCGLE results actually reflect the tentative definition of  $t^{eq}$  proposed in Ref. [49], rather than a poor accuracy of the NE-SCGLE predictions for  $\tau_\alpha(t)$ , as we confirmed by exploring other definitions of  $t^{eq}$ .

Thus, inspired by reference [28] we finally adopted the use of the apparent instantaneous slope  $\mu(t)$  to determine  $t^{eq}$ . Specifically, in terms of this quantity the equilibration condition is defined as  $\mu(t^{eq}; T_f) = 0.1$ . Analyzing the NE-SCGLE data for  $\tau_\alpha(t)$  in Fig. 2(f) with this new criterion, we determined the solid black circles in the figure, which align themselves according to the empirical fit  $\tau_\alpha^{eq}(T_f) \approx 0.189 \times [t^{eq}(T_f)]^{0.795}$ , which implies that  $t^{eq}(T_f) \propto [\tau_\alpha^{eq}(T_f)]^{1.26}$ , now in full agreement with simulations. For completeness, we also reanalyzed the quench processes studied in Ref. [49], now applying this new definition of  $t^{eq}$ , with the result  $\eta = 1/\gamma = 1/0.92 = 1.08$ .

Regarding other features of the simulations that are consistently described by the theory, let us stress that the apparent instantaneous slope  $\mu(t)$  of the latter is also smaller than the slope of the dashed straight line of the figure, and that the apparent instantaneous slope  $\mu(t)$  first increases with  $t$ , and beyond an inflection point, it decreases. Furthermore, as in the simulations, for deeper quenches, this inflection point also becomes a finite interval in which  $\tau_\alpha(t)$  increases as a power law of  $t$ ,  $\tau_\alpha(t) \propto t^\delta$ , with  $\delta < 1$ . Thus, in conclusion, theory

and simulations agree in the general physical scenario for the equilibration processes of the instantaneously quenched WCA liquid.

#### IV. AGING OF A QUENCHED SOFT-SPHERE SYSTEM.

We now discuss the other possible scenario for the irreversible relaxation of the WCA model, in which the system starts at the same initial equilibrium state as before, but is now quenched into the non-ergodic region (i.e.,  $T_f \leq T^a(\phi = 0.7)$ ) where it is predicted to become dynamically arrested. In Fig. 3 we summarize the results obtained with BD simulations (upper panels) and the NE-SCGLE (lower panels) for three representative quenches at the indicated temperatures.

##### A. Aging of the structure and dynamics of the WCA model: Brownian dynamics.

As shown in Fig. 3(a), for a deeper quench of the simulated system ( $T_f = 0.1$ ) the SF exhibits what at first sight seems essentially the same qualitative time-evolution as that found for the equilibration process described in Fig. 2(a) (for  $T_f = 0.25$ ). As before, this evolution consists of a gradual increase of the structural correlations around the same wave vector number  $k = k_{max}$  and the development of a (rather similar) stationary SF. A noteworthy difference with respect to the case of equilibration, however, is observed in the much slower relaxation of  $S(k;t)$  towards a stationary value. One notices, for instance, that the time scale required to reach stationarity now extends over virtually the whole waiting time-window resolved in our BD simulations (see the inset of Fig. 3(a)) and, also, that such time scale becomes roughly two orders of magnitude larger with respect to that described in the inset of Fig. 2(a). Thus, upon a deeper quench, except for the much slower relaxation of the SF to acquire a new stationary value, the function  $S(k;t)$  does not exhibit any other obvious qualitative difference with respect to an equilibration process.

This is to be contrasted with the dynamical behavior shown in Fig. 3(b), which is fundamentally different from that of Fig. 2(b) describing the equilibration of the dynamics. In this case, for example, one notices a more pronounced slowing down in the simulated system, highlighted by the gradual development of a plateau in  $F(k;t)$  that leads to a much larger increase of  $\tau_\alpha(t)$  at comparable waiting-times (up to two orders of magnitude). More

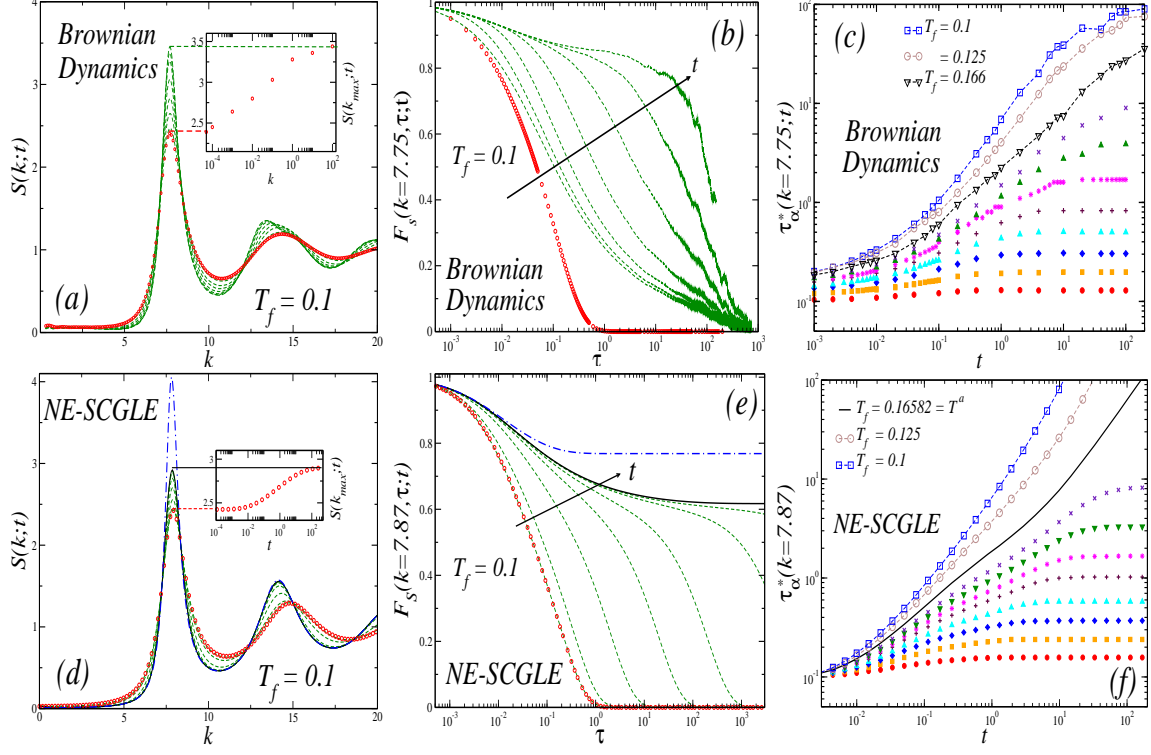


FIG. 3. Schematic representation of an aging process of the WCA fluid after an instantaneous isochoric quench from the equilibrium state ( $\phi = 0.7, T_i = 1$ ) towards a final temperature  $T_f$  below the dynamical arrest point  $T^a = 0.166$ . (a) and (b) Sequence of snapshots at waiting times  $t = 10^{-3}, 10^{-2}, 10^{-1}, 10^0, 10^1, 10^2$  and  $10^3$  (green dashed lines) obtained from BD simulations describing the  $t$ -evolution of  $S(k;t)$  and  $F(k, \tau; t)$ , respectively, after an instantaneous quench to  $T_f = 0.1$ . In both figures, the initial ( $t = 0$ ) values are indicated in open symbols. (c) Evolution of  $\tau_\alpha^*(t)$  for three different quenches below the dynamic arrest temperature as indicated (dashed lines with open symbols). For reference, we show again the data of Fig. 2(c) (solid symbols). (d) and (e) Sequence of snapshots at waiting times  $t = 10^{-3}, 10^{-2}, 10^{-1}, 10^0, 10^1, 10^2$  and  $10^3$  (green dashed lines) obtained with the NE-SCGLE for  $S(k;t)$  and  $F(k, \tau; t)$ , respectively, for a quench with  $T_f = 0.1$ . In these figures, the solid lines represent the arrested values  $S^a(k)$  and  $F_S^a(k, \tau)$ , whilst the dashed-dotted lines correspond to the thermodynamical input  $[n\mathcal{E}^{(f)}(k)]^{-1}$  and the prediction of the equilibrium SCGLE for  $F^S(k, \tau : t \rightarrow \infty)$  (see the text). (f) Evolution of  $\tau_\alpha^*(t)$  for a quench to the critical value  $T^a(\phi = 0.7) = 0.16582$  (solid line) and for two additional aging processes (symbols with solid-lines) predicted by the NE-SCGLE for quenches inside the region of dynamical arrest. For reference, we show again the data of Fig. 2(f) (solid symbols).

crucially, for this quench the  $\alpha$ -relaxation time does not exhibit any evidence of stationarity within the waiting-time window of the simulations and, instead, it continues increasing with  $t$ . These features are reminiscent of an aging process in the dynamics [25, 28], where the characteristic relaxation time (and, hence, the viscosity of the system) increases dramatically and persistently with system's age during the endless process of formation of a glassy state.

From the comparison of Figs. 2(a) and 2(b) with Figs 3(a) and 3(b), respectively, one notices that two different quenches with rather similar stationary structural correlations display an entirely different dynamical behavior, which is indicative of the crossover from the equilibration to the glassy regime. To emphasize such crossover, Fig. 3(c) exhibits the simulation results for the aging of the  $\alpha$ -relaxation time corresponding to three representative quenches with final temperatures below the dynamical arrest temperature (open symbols with dashed lines). For reference, Fig. 3(c) also reproduces the results for  $\tau_\alpha(t)$  of the equilibration processes in Fig. 2(c) (solid symbols), thus highlighting the transition from the previously discussed pattern of equilibration, where  $\tau_\alpha(t)$  saturates to the value  $\tau_\alpha^{eq}(T_f)$  after an equilibration time  $t^{eq}(T_f)$ , to a characteristic pattern of aging. In the latter,  $\tau_\alpha(t)$  displays a notoriously larger and unbounded growth, with no equilibration time identifiable within the waiting time window of the simulations. Instead, what we observe is an increasingly longer time interval in which  $\tau_\alpha(t)$  grows as  $\tau_\alpha(t) \propto t^\delta$ , with a sub-aging exponent that gradually approaches the unity value as  $T_f$  becomes smaller (see Sec. IV D). Beyond this interval, the aging effects on the dynamics become more sensitive on the observation time window, so that the evolution of the structural relaxation time is no longer described by a simple power law and follows, instead, and approximate functional relationship of the form  $\tau_\alpha(t) \propto t^\mu$ , with  $\mu(t) = \mu[t; T_f]$  being the apparent instantaneous slope introduced in Sec. III.

### B. Aging of the structure of the WCA model: NE-SCGLE theory.

All the above mentioned non-equilibrium fingerprints observed in the kinetics of the structure and dynamics of the simulated system can be well understood within the framework of the NE-SCGLE. To see this, let us refer first to the most central equation of this theory, namely, Eq. (A1) in appendix A, which describes the time-evolution of the SF after a quench towards a final state point  $(n_f, T_f)$  and reads



$$\frac{\partial S(k; t)}{\partial t} = -2k^2 D^0 b(t) n_f \mathcal{E}^{(f)}(k) [S(k; t) - 1/n_f \mathcal{E}^{(f)}(k)].$$

In this equation the mobility function  $b(t) = D^L(t)/D^0$  is given in terms of the long-time self-diffusion coefficient  $D^L(t)$  (at observation time  $t$ ) and  $\mathcal{E}^{(f)}(k)$  is the second functional derivative of a postulated Helmholtz free energy density-functional, evaluated at the uniform (bulk) density and temperature fields  $n(\mathbf{r}, t) = n_f$  and  $T(\mathbf{r}, t) = T_f$ . As explained in detail in Refs. [47–49], this externally determined thermodynamical input plays a fundamental role in the NE-SCGLE description of glassy states, with  $[n_f \mathcal{E}^{(f)}(k)]^{-1} = S^{eq}(k)$  actually being the equilibrium structure factor at the state point  $(n_f, T_f)$ . The function  $n_f \mathcal{E}^{(f)}(k)$  can also be written as  $n_f \mathcal{E}^{(f)}(k) = 1 - n_f c[k; n_f, T_f]$ , with  $c[k; n_f, T_f]$  being the Fourier transform of the two-particle direct correlation function [65].

Thus, in connection with the previous discussion, let us consider the stationary solutions ( $\partial S(k, t)/\partial t = 0$ ) of the above equation, which might be classified in two different categories by mere inspection. The first category are equilibrium solutions, occurring for quenches with  $T_f > T^a$  and determined by the condition  $[S(k; t) - 1/n_f \mathcal{E}^{(f)}(k)] = 0$ , which implies that  $S(k; t)$  indeed attains its equilibrium expected value  $S^{eq}(k) = 1/n_f \mathcal{E}^{(f)}(k)$  within a finite waiting-time window. The specific kinetic features of this kind of solutions were already discussed and highlighted in the three lower panels of Fig. 2, finding a remarkable consistency with the results of BD. This includes the same essential evolution of the SF within a comparable time-window, and the commensurable slowing down of the microscopic dynamics. More important, however, it also includes the rather similar power law predicted for the equilibration time-scale of the WCA model. Thus, equilibrium solutions are one of the possible stationary solutions of Eq. (A1).

A second category of stationary solutions, however, are those describing dynamical arrest, corresponding to quenches inside the non-ergodic region, or  $T_f \leq T^a$ . In this case, the condition  $\partial S(k; t)/\partial t = 0$  is fulfilled because the function  $b(t)$  (that is, the diffusivity of the constituent particles) decreases dramatically with  $t$  (ideally vanishing at  $t = \infty$ ). This leads to a different kind of stationarity in the SF, that originates in underlying kinetic barriers and, hence, does not require the equilibrium condition  $\lim_{t \rightarrow \infty} S(k; t) = S^{eq}(k)$  to be satisfied. This kind of solutions happens to correspond to glasses, gels, and other non-equilibrium amorphous states, as it has been systematically illustrated in very specific circumstances in the context of glass-forming systems whose particles interact through repulsive [49–51],

attractive [52–54] and even non-spherical potentials [68, 69]. For this scenario, the function  $S(k; t)$  is predicted to evolve with waiting-time towards a new stationary value  $S_a(k)$  which, as revealed by the NE-SCGLE, is fundamentally different from the equilibrium structure factor  $S^{eq}(k)$ .

The importance of emphasizing this fundamental distinction can hardly be overstated. A noteworthy reason is that, as seen in the simulation results of Figs. 2(a) and 3(a), the difference between the stationary values attained by  $S(k; t)$  for equilibration or dynamical arrest is, for all practical purposes, indistinguishable. This, for instance, might complicate – or even impede – to experimentally distinguish between equilibration and non-equilibrium aging at the level only of the static structural correlations represented by  $S(k; t)$  (excepting for the much slower relaxation to reach a stationary value in the later case) Within the NE-SCGLE framework, in contrast, such distinction is explicitly recognized through the intrinsic difference between the predicted arrested value  $S_a(k)$  (which, in general, depends on the protocol of fabrication) and the equilibrium structure factor  $S^{eq}(k)$ . It is worth mentioning here that such difference is generically enhanced as  $T_f$  decreases [69] (always below the critical temperature  $T^a$ ).

To provide a more vivid notion of these concepts, let us now refer to Fig. 3(d) which displays the arrested kinetics of the SF as described by the NE-SCGLE for a quench with  $T_f = 0.1 < T^a(\phi = 0.7) = 0.16582$ . As observed before when comparing the simulation results of Figs. 3(a) and 2(a), the theoretically predicted results for  $S(k; t)$  in Fig. 3(d) also describe a qualitatively similar evolution compared to that obtained for the equilibration process shown in Fig. 2(d). Also in agreement with our BD simulations, this relaxation takes place during a larger time-scale, after which  $S(k; t)$  saturates to the stationary value  $S_a(k)$ . This non-equilibrium stationary SF, highlighted by the solid line in Fig. 3(d), is notably different from the equilibrium structure factor  $S^{eq}(k) = 1/n_f \mathcal{E}^{(f)}(k)$  expected at the final state, included for reference in the same figure (dashed-dotted line). Hence, according to our previous discussion, this indicates that the stationarity in  $S(k; t)$  originates in the dynamical arrest conditions imposed by the long-time vanishing of the mobility  $b(t)$ .

### C. Aging of the dynamics of the WCA model: NE-SCGLE theory.

Besides the previously described non-equilibrium kinetics of the SF, the NE-SCGLE also provides predictions for the aging of the dynamics. In Fig. 3(e), for example, we show the theoretical results obtained for the  $t$ -evolution of the ISF after a quench with  $T_f = 0.1$ . Clearly, these results exhibit the same qualitative features as those reported by the simulations in Fig. 3(b). For instance, one notices that the theory also predicts an aging process, characterized by the development of an increasingly long-lasting plateau in the function  $F^S(k, \tau; t)$  and leading to a persistent growth of  $\tau_\alpha(t)$  with  $t$ . In other words, the results of both simulations and theory support the interpretation that, at any *finite* waiting-time  $t$ , the self ISF will always decay to zero with  $\tau$  after a *finite*  $\alpha$ -relaxation time  $\tau_\alpha(t)$ , in full agreement also with experimental data on glass forming liquids. This qualitative consistency between theory, simulations and experiments, however, is restricted by the practical limit of the longest possible waiting times that are accessible in any simulation and/or experiment.

The NE-SCGLE, however, still has meaningful predictions beyond such practical limitation, even if simulations or experiments cannot wait long enough to test them. For instance, the theory assures us that, at any finite waiting time  $t$  beyond the aforementioned practical limit, the ISF will continue to decay to zero after a *finite*  $\alpha$ -relaxation time  $\tau_\alpha(t)$ , regardless of the fact that we cannot measure such decay. It is only at the ideal asymptotic limit  $t = \infty$ , that  $F_S(k, \tau; t)$  is predicted to never decay with  $\tau$  (solid line in Fig. 3(e)). Therefore, the theory itself advises that such idealized physical scenario is, for obvious reasons, unobservable in practice. This decoupling between the theoretical predictions of equilibrium approaches such as MCT and the SCGLE, and experimental or simulated observations, originates in the extremely slow kinetics of the aging processes that are characteristic of glass formation, as compared with the kinetics of equilibration, which always relaxes within finite equilibration times (except in the close vicinity of  $T^a$ ).

This realistic NE-SCGLE aging scenario thus complements and clarifies some fundamental aspects of the notion of the “ideal glass transition” predicted by both MCT and the SCGLE [46]. Recall that these theories only provide the equilibrium value  $F_S^{eq}(k, \tau)$  of the ISF at any state point  $(\phi, T)$ , without any mention to the waiting time  $t$ . For reference, in Fig. 3(e) we also show the prediction of the equilibrium SCGLE theory for  $F_S^{eq}(k, \tau)$ , calculated at the (arrested) state point  $(\phi = 0.7, T_f = 0.1)$  (dash-dotted line). These equilibrium

dynamical correlations involve an infinitely-lasting plateau, thus illustrating the MCT-like prediction that  $\tau_\alpha^{eq}(\phi, T)$  is infinite (or equivalently,  $D^L = 0$ ) for  $T \leq T^a(\phi)$ . However, in the more general framework of the NE-SCGLE theory  $F_S^{eq}(k, \tau)$  is only one possible asymptotic long-time limit of the function  $F_S(k, \tau; t)$ , *i.e.*,  $F_S^{eq}(k, \tau) = F_S(k, \tau; t \rightarrow \infty)$ . In addition, for  $T_f \leq T^a(\phi)$  another long-time asymptotic limit  $F_S^a(k, \tau)$  exists (solid line in Fig. 3(e)), representing non-equilibrium dynamically arrested states. Although both limits exist and compete, the spontaneous kinetic evolution after quenching favors the gradual development of the dynamically arrested limit  $F_S^a(k, \tau)$ . In contrast, for  $T_f > T^a(\phi)$ , neither  $S_a(k)$  nor  $F_S^a(k, \tau)$  exist, but  $S^{eq}(k)$  and  $F_S^{eq}(k, \tau)$  do, leaving the system with only one possibility, namely, to equilibrate.

Let us stress that there is a complete coincidence between the NE-SCGLE theory and its equilibrium (SCGLE) version, regarding the existence and location of the “ideal” glass transition line  $T = T^a(\phi)$  (solid line in Fig. 1). As explained in Refs. [47–49], the predicted value of the critical temperature  $T^a(\phi)$  turns out to coincide exactly with the critical temperature predicted by the equations of the equilibrium SCGLE theory. This is probably not that remarkable, since the NE-SCGLE theory is a natural non-equilibrium extension of this equilibrium theory (and, disregarding details, of MCT [46]). Thus, one might be tempted to extend the same criticism originally made to MCT, regarding the non-observability of this predicted “ideal” glass transition line, to the NE-SCGLE theory. In the light of the present discussion, however, it is clear that this criticism doesn’t apply in the present case, since the genuinely relevant comparison is between the real experimental measurements of  $F_S(k, \tau; t)$  and  $\tau_\alpha(t)$  at finite waiting times, and their theoretical counterparts, provided only by the NE-SCGLE theory.

This is illustrated here with the results in Fig. 3(f), which display the behavior of  $\tau_\alpha(t)$  as predicted by the NE-SCGLE for the same sequence of simulated instantaneous isochoric quenches in Fig. 3(c). These quenches start from the same initial temperature  $T_i$ , and end at final temperatures  $T_f$  falling above (solid symbols), at (solid line), and below (open symbols with dashed lines) the theoretically-determined dynamical arrest temperature  $T^a(\phi = 0.7) = 0.166$ . Just like the simulation results in Fig. 3(c), these theoretical predictions also illustrate the passage from the characteristic pattern of equilibration ( $T_f > T^a$ ) to the dynamical arrest regime ( $T_f \leq T^a$ ). Thus, according to the more realistic theoretical lens provided by the NE-SCGLE theory, the discontinuous dynamical arrest transition predicted by MCT and

the equilibrium SCGLE theory actually appears, at any realistic finite waiting time  $t$ , as a broad crossover from full equilibration to full dynamic arrest. These are relevant issues that deserve to be discussed further, as we do in the Section V. Before doing so, however, we find useful to provide first a stringent comparison of theory and simulations.

#### D. Comparison of simulations and theory

The results in Figs. 3(c) and 3(f) are highly instructive and revealing since, combined, they provide a consistent kinetic description of the isochoric processes of equilibration and aging occurring in the WCA liquid. To better compare theory and simulations at realistic waiting times, in Fig. 4(a) we plot together such results. There we can observe the remarkable quantitative agreement at all waiting times in the equilibration regime ( $T_f > T^a = 0.166$ ). For the three quenches with  $T_f \leq T^a$  (i.e., in the dynamic arrest regime), theory and simulations also coincide in predicting a stronger slowing down of the dynamics, represented by an increasingly faster development of  $\tau_\alpha(t)$ .

In both, the equilibration and dynamical arrest scenarios, one also observes an excellent semi-quantitative agreement at intermediate waiting times. As mentioned above, in this  $t$ -regime  $\tau_\alpha(t)$  grows as a power law of  $t$ ,  $\tau_\alpha(t) \propto t^\delta$ , with a  $T_f$ -dependent sub-aging exponent  $\delta < 1$ . The emergence of this sub-aging regime is better illustrated in Fig. 4(b), which considers three representative quenches above ( $T = 0.25$ ), at ( $T = 0.166$ ) and below ( $T_f = 0.1$ ) the critical value  $T^a$ . For reference (and to serve as a guide for the eye) in the same figure we also plot three different power laws in thick dashed lines, obtained from a fit of the simulated data for  $t \in [10^{-1}, 10^1]$  and which highlight the remarkable coincidence of theory and simulations at intermediate  $t$ . Notice that, in both approaches,  $\delta \rightarrow 1$  as  $T_f$  becomes smaller.

For quenches with  $T_f \leq T^a$ , however, the agreement of theory and simulations visibly deteriorates at longer  $t$ , with the theoretical  $\tau_\alpha(t)$  growing even faster, as an asymptotic power law  $\tau_\alpha(t) \propto t^\gamma$ , with  $\gamma > 1$  (hyper-aging) for the two quenches with  $T_f < T^a$ , and with  $\gamma = 1$  (normal aging) for the quench to the critical temperature  $T^a = 0.166$  [73]. As seen in Fig. 4(b), the simulation results strongly deviate from this predicted asymptotic behavior. The origin of these deviations, however, is not difficult to understand. Although there may be a variety of reasons, the most relevant ones we can think of, are the deviations

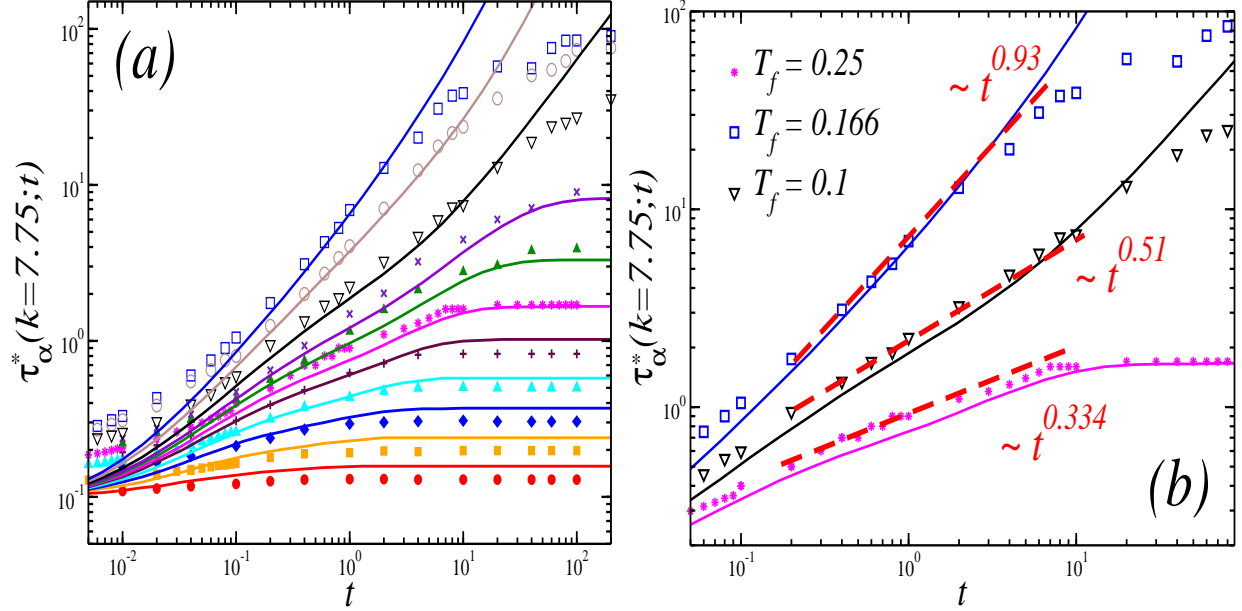


FIG. 4. (a) Comparison of the results in Figs. 3(c) and 3(f) for  $\tau_\alpha^*(k; T_f; t)$ , as a function of waiting time  $t$ . Symbols correspond to simulation results, with the same nomenclature used in Fig. 3 for the  $T_f$ -values of the sequence of quenches, whereas lines describe the corresponding results of the NE-SCGLE shown in Fig. 3(f). Same information as in (a), but only for the three representative quenches above ( $T_f = 0.25$ ), at ( $T_f = T^a = 0.166$ ) and below ( $T_f = 0.1$ ) the ideal glass transition temperature  $T^a = 0.166$ . The thick dashed lines describe power laws of the form  $\tau^\alpha \sim t^\delta$ , with exponent (from bottom to top)  $\delta = 0.334, 0.51, 0.93$ , obtained from a fit of the simulation data for  $t \in [10^{-1}, 10^1]$  (see the text).

$\Delta \bar{n}(\mathbf{r}; t) \equiv \bar{n}(\mathbf{r}; t) - n$  of the local mean particle density  $\bar{n}(\mathbf{r}; t)$  from its bulk value  $n$ . These deviations describe the spatial heterogeneity of the local density and, consequently, the emergence of dynamical heterogeneities, unavoidably present in microscopic simulations and in real experiments.

The original and most general version of the NE-SCGLE theory, summarized by Eqs. (4.1)-(4.7) of Ref. [47], was posed precisely in terms of the time-evolution equations for the mean value  $\bar{n}(\mathbf{r}, t)$  and covariance  $\sigma(\mathbf{r}, \mathbf{r}'; t)$ , of the instantaneous local particle density  $n(\mathbf{r}, t)$  of the fluid (see Eqs. (4.1)-(4.3) of Ref. [47]). The solution of such time-evolution equations, which are coupled between them through a state-dependent local mobility function  $b(\mathbf{r}, t)$ , in principle include the description of these spatial (structural and dynamical) heterogeneities. Unfortunately,  $b(\mathbf{r}, t)$  must be determined by a self-consistent system of

equations (Eqs. (4.4)-(4.7) of Ref. [47]), which involve spatially-varying non-equilibrium dynamical properties. The numerical solution of the resulting full system of equations poses a formidable technical challenge.

To have a glimpse of the physical scenario revealed by this general non-equilibrium theory, however, a provisional simplification was introduced [47], in which one solves these equations ignoring precisely these spatial heterogeneities. For this, we neglect the deviations  $\Delta\bar{n}(\mathbf{r}; t)$ , in which case  $\bar{n}(\mathbf{r}; t) = n$ , and hence, we do not need the time evolution equation for  $\bar{n}(\mathbf{r}; t)$  (Eq. (4.1) of Ref. [47]). Within this approximation, Eqs. (4.3)-(4.7) of Ref. [47] become Eqs. (A1)-(A5) of Appendix A, which are precisely the equations representing the simpler version of the NE-SCGLE theory employed in the present study. Clearly, to go beyond this level of approximation we would need some strategy to incorporate the deviations  $\Delta\bar{n}(\mathbf{r}; t)$ . The resulting  $\bar{\tau}_\alpha(t)$  is expected to agree with the simulations in exhibiting similar deviations from the simplified theoretical behavior described by the solid lines of Fig. 4(a).

Implementing this or other strategy to incorporate spatial heterogeneities in the NE-SCGLE description is, however, not the main focus of the present paper, which is aimed, instead, at exhibiting how accurately the simpler current version of the NE-SCGLE theory agrees with the simulated aging of the system in the realistic regime of short and intermediate times. In the meanwhile, however, let us mention that the generic behavior of the simulation results in Fig. 4 regarding their long-time deviations from theory, can also be understood from a rigorous mathematical analysis of the solutions of the NE-SCGLE equations following, to a large extent, the steps of Ref. [46] for the asymptotic solutions of the equilibrium SCGLE theory. Such an analysis allows to identify the *closeness* of the structural relaxation for “arbitrary”  $T_f$  in terms of an expansion parameter  $\sigma = |1 - (T_f/T^a)|$  (with  $\sigma \ll 1$ ). The resulting theoretical scenario includes the prediction of the asymptotic normal and hyper-aging regimes of the dynamics for, respectively,  $T_f = T^a$  and  $T_f < T^a$ . Although in practice these asymptotic regimes are interrupted by the spatial heterogeneities, the emerging dynamical heterogeneities can also be taken into account by merging the NE-SCGLE approach with the recently developed stochastic  $\beta$ -relaxation theory [71, 72], with the former allowing to include non-mean-field fluctuations which account for the aforementioned deviations in the long  $t$  regime. A thorough discussion of these aspects can be consulted in Ref. [73].

## V. UNIVERSAL CROSSOVER FROM EQUILIBRATION TO AGING.

Let us now focus on our main objective of emphasizing the strengths of the current version of the theory, even without including heterogeneities. In this sense, perhaps the farthest-reaching prediction of the simplified NE-SCGLE equations (A1)-(A6), is the existence of the critical temperature  $T^a(\phi)$  that separates the two possible (and mutually exclusive) physical scenarios of equilibration (when  $T_f > T^a(\phi)$ ) and aging (when  $T_f < T^a(\phi)$ ). The existence of this critical temperature  $T^a(\phi)$  was first predicted by MCT (and later also by the equilibrium SCGLE theory), but only referring to the long-time asymptotic regime. The NE-SCGLE theory extends this prediction to any finite time after the quench, thus providing a richer and more explicit conceptual scenario, that can be employed to understand the phenomenology of the aging of real and simulated materials, severely constrained by the finite time-span of practical observations. In fact, the solution of these equations yields the time-evolution of the most relevant properties ( $S(k; t)$ ,  $b(t)$ ,  $F_S(k; \tau; t)$ ,  $\tau_\alpha^*(t, T_f)$ , etc.) at *any finite* waiting times, starting from the experimentally accessible short and intermediate times, to the often inaccessible asymptotically long times.

In order to illustrate these concepts more clearly, let us now present the same information in Fig. 4(a), but now in a complementary format, by plotting  $\tau_\alpha^*(t; 1/T_f)$  as a function of the inverse temperature  $1/T_f$  for a sequence of fixed waiting times. Fig. 5(a) displays such information, which shows that simulations and theory agree in reporting two distinct regimes as a function of  $1/T_f$  in these plots. To see this, notice that each theoretical curve for  $\tau_\alpha^*(t; 1/T_f)$  at fixed waiting time  $t$ , exhibits a regime corresponding to samples that, at time  $t$ , have fully equilibrated ( $1/T_f \leq 1/T_0(t)$ ), followed by a second regime, corresponding to samples that have not yet reached equilibrium ( $1/T_f \geq 1/T_0(t)$ ). These two regimes are separated by a crossover inverse temperature  $1/T_0(t)$ , highlighted by the black solid circles in the figure. Focusing on the simulation results for  $t = 10^1$ , for instance, we find a crossover value  $1/T_0(t = 10^1) \approx 4.13$  (i.e.,  $T_0(t = 10^1) \approx 0.242$ ), whereas for  $t = 10^2$  we find  $1/T_0(t = 10^2) \approx 5.21$  ( $T_0(t = 10^2) \approx 0.192$ ). One notices that the crossover  $[1/T_0(t)]$  found in simulations first increases rather fast with  $t$  and then tends to saturate, with the crossover points following closely the ideal curve  $\tau_\alpha^{(eq)}(1/T)$  (dashed line) predicted by the equilibrium SCGLE theory, which diverges as  $T$  approaches the critical value  $T^a = 0.16582$ . The theoretical prediction is that  $[1/T_0(t)] \rightarrow [1/T^a]$  from below (i.e.,  $T_0(t) \rightarrow T^a$  from



above) as  $t \rightarrow \infty$ , which is the trend confirmed through the duration ( $t \leq t_{max} \approx 10^2$ ) of our simulations. The results in Fig. 4(a) then illustrate the origin of the un-observability of any divergence of  $\tau_\alpha^*(t)$  in our BD simulations, particularly for quenches with  $T_f$  well below the critical temperature  $T^a$ . In fact, the theoretical prediction is that the same scenario will prevail no matter how long the simulations (or experiments!) last, since they will always involve finite waiting times.

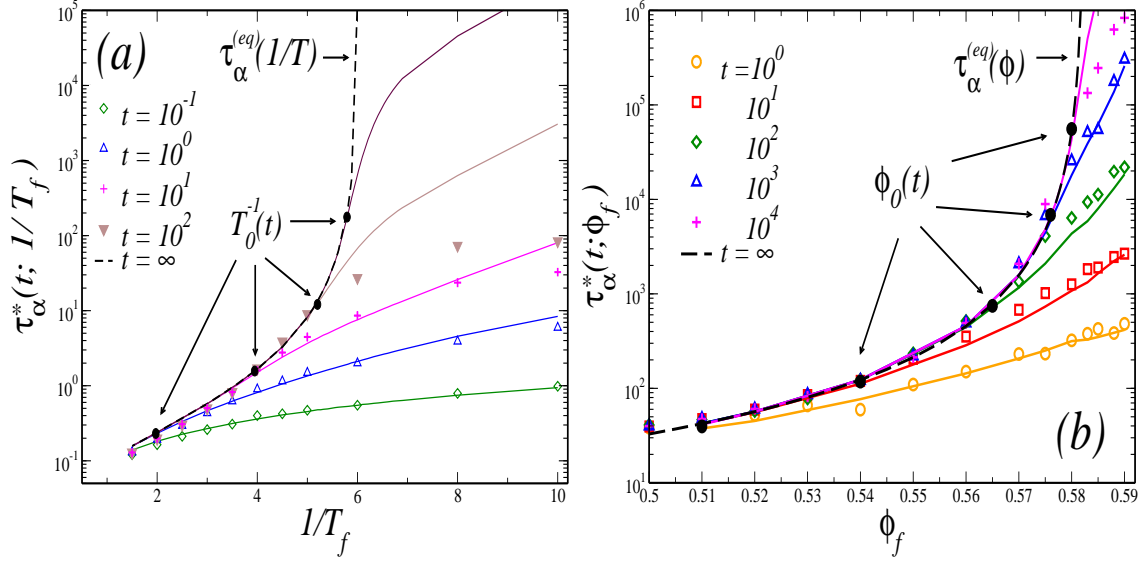


FIG. 5. (a) Same information of Figs. 3(c) and 3(f) for the  $\alpha$ -relaxation time  $\tau_\alpha^*(k; T_f; t)$ , but now displayed as a function of the inverse temperature  $1/T_f$  at fixed waiting time  $t$ , as indicated. Symbols are used for the simulation data whereas lines correspond to the results of the NE-SCGLE. The black solid circles highlight the crossover value  $1/T_0(t)$  that separates samples which have equilibrated from those which are insufficiently equilibrated, for distinct waiting times (see the text). The dashed line corresponds to the prediction of the equilibrium SCGLE for  $\tau_\alpha^{(eq)}(k; 1/T)$ . (b) Molecular dynamics simulation data (symbols) and theoretical results (solid lines) reported in Ref. [51] for the volume fraction dependence of  $\tau_\alpha^*(k; \phi_f; t)$  at different waiting times, as indicated, for quenches of the WCA model to a final temperature  $T_f = 0$  and approaching the critical value  $\phi_{HS}^a$ . As in (a), the dashed line corresponds to the prediction of the SCGLE for  $\tau_\alpha^{(eq)}(k; \phi)$ .

In fact, essentially the same physical scenario was found in Refs. [50, 51] in considerably longer molecular dynamics simulations of a sequence of quenches of the WCA model to the final temperature  $T_f = 0$ , but along a sequence of isochores with increasing volume fraction  $\phi$ . This was used to investigate the density-driven hard-sphere glass transition of the HS

model by increasing the volume fraction  $\phi_{HS}$  towards its critical value  $\phi_{HS}^a = 0.582$ . To serve as a reference, in Fig. 4(b) we reproduce the plot of  $\tau_\alpha^*(t; \phi_f)$  vs  $\phi_{HS}$  at different waiting times, extracted from Fig. 3 of Ref. [51], which compared molecular dynamics (MD) simulations and theory. Just as in Fig. 4(a), one observes that for quenches with  $\phi_{HS} \geq 0.582$  the  $t$ -dependent  $\alpha$ -relaxation time does not saturate to its equilibrium value within the total duration of the MD simulation runs. Therefore, in both cases (Figs. 4(a) and 4(b)) the comparison between the results of simulations of duration  $t_{max}$  and the predictions of equilibrium theories, such as SCGLE or MCT, is only meaningful for samples below the crossover thresholds  $1/T_0(t_{max})$  and  $\phi_0(t_{max})$ , respectively.

Let us also emphasize that the noticeable qualitative similitude of the overall physical scenario outlined by Figs. 4(a) and 4(b), along with all the results presented so far, provides a vivid confirmation of the intuitive notion that the inverse temperature  $1/T$  plays an analogous role to that of the volume fraction  $\phi$  in determining the structural relaxation of the WCA model near the glass transition. We should stress here that this physical notion is also in agreement with experimental data for soft-sphere colloidal suspensions approaching the GT upon variations in both parameters [59]. In addition, let us mention that a full correspondence between the two control parameters may also be established more explicitly when extending to non-equilibrium conditions the principle of dynamic equivalence between soft- and hard-sphere fluids [70]. Such discussion, however, is out of the scope of the present contribution and is left for further work.

## VI. CONCLUDING REMARKS

In summary, in this work we have combined Brownian dynamics simulations and NE-SCGLE theoretical calculations to present a consistent physical description of the irreversible isochoric relaxation of a soft-sphere glass-forming liquid suddenly quenched towards conditions of dynamical arrest. Such relaxation was analyzed in terms of the structural and dynamical properties of the model liquid, whose waiting time evolution falls in two mutually exclusive possibilities: either the system equilibrates within a finite equilibration time-scale  $t^{eq}(T_f)$  that depends on the final temperature of the quench, or the system becomes dynamically arrested and ages endlessly during the process of becoming a glass.

The distinction between these two scenarios was based on the theoretical predictions of

the dynamical behavior of the liquid after quenching. The evolution of the  $\alpha$ -relaxation time  $\tau_\alpha(t)$ , in particular, allowed for the description of the crossover from the equilibration to the aging regimes, and to highlight various non-equilibrium fingerprints that characterize the relaxation of the model system studied. In the case of equilibration (that is, for quenches above the critical temperature,  $T_f > T^a$ ), both,  $\tau_\alpha^{eq}(T_f)$  and the equilibration time  $t^{eq}(T_f)$  required to reach thermodynamic equilibrium, are found to remain finite, with  $t^{eq}(T_f)$  growing as a power law of  $\tau_\alpha^{eq}(T_f)$  and with both quantities showing a significant increase as  $T_f$  approaches  $T^a$  from above. For quenches to  $T^a$  or below, instead,  $\tau_\alpha(t)$  undergoes a persistent growth with system's age within the whole waiting-time resolution employed, showing also an increasingly faster growth for smaller  $T_f$ . These dynamic features were consistently found in our simulations and in the predictions of the non-equilibrium self-consistent generalized Langevin equation theory.

At the level of structural correlations, in contrast, the two relaxation scenarios turn out to be very similar and, therefore, too difficult (if not impossible) to distinguish in the simulations. For both, equilibration and dynamical arrest, the static structure factor evolves towards a stationary value which does not exhibit any noticeable qualitative difference. The theoretical framework employed here, however, has shown to provide a powerful microscopically founded tool for the understanding of the two relaxation processes at the level of both, the dynamical and the structural properties. In the latter case, for instance, the theory explicitly recognizes and emphasizes the fundamental differences between equilibration and dynamical arrest in terms of the predicted long time asymptotic limit of  $S(k; t)$  which, for equilibration, reaches its thermodynamic equilibrium value  $S^{eq}(k)$ , while for dynamical arrest attains a non-equilibrium (and theoretically well defined) arrested value  $S^a(k)$ . As explained in Sec. [IV B](#), despite the misleading quantitative similarity between  $S^{eq}(k)$  and  $S^a(k)$ , the intrinsic difference between these stationary values plays a fundamental role in determining the dynamical behavior of the system. The theory highlights such difference from the very beginning through its most central equation, which relates the mobility of the constitutive particles with the stationary values through a highly non-linear functional dependence.

In our present contribution we have demonstrated the qualitative equivalence between the packing fraction and the inverse temperature as control parameters determining the non-equilibrium relaxation of a soft-sphere liquid. Furthermore, our results provide convincing

evidence of the universality of the aging exponents accounting for the slowing down of the dynamics in systems described by short-range stiff potentials, as compared to independent simulation results [28].

Despite the various approximations adopted at the level of structure and dynamics for the theoretical description of the WCA liquid, the qualitative and semi-quantitative agreement between theory and simulations provides a rigorous validation of the non-equilibrium self-consistent generalized Langevin equation approach as a fundamental tool for the understanding of dynamical arrest phenomena in thermally driven glass-forming liquids. Thus, we expect that the methodology and analysis presented in this work could serve as a benchmark for the study and characterization of glass formation in more complex systems involving, for instance, mixtures of thermo sensitive particles, fluids involving anisotropic (e.g., dipole-dipole) interactions [68, 69], and even more complex conditions.

**ACKNOWLEDGMENTS:** LFEA and FPV acknowledge the Consejo Nacional de Ciencia y Tecnología (CONACYT, México) for support through a Postdoctoral Fellowship (Grant No. I1200/224/2021). MMN, RPO, ELL, MCP and HRE are also grateful to CONACYT for financial support through grants No. 320983, CB A1-S-22362, No. CF-2019-731759, and LANIMFE 314881.

**DATA AVAILABILITY:** The data that support the findings of this study are available from the corresponding author upon reasonable request.

## Appendix A: Theoretical considerations.

In this appendix we summarize the essence of the simplified NE-SCGLE theory used to investigate the relaxation of the WCA model system.

### 1. Review of the NE-SCGLE theory.

The NE-SCGLE theory was first derived in Ref. [47] and is summarized by a set of coupled time-evolution equations, whose solution (for  $t > 0$ ) describes the irreversible relaxation of an instantaneously quenched liquid. The most central of these equations describes the waiting-time evolution of the static structure factor  $S(k, t)$ . For an homogeneous system, instantaneously quenched at  $t = 0$  from an initial equilibrium state  $(n_i, T_i)$  and towards a final state  $(n_f, T_f)$ , such equation reads

$$\frac{\partial S(k; t)}{\partial t} = -2k^2 D^0 b(t) n_f \mathcal{E}(k; n_f, T_f) [S(k; t) - 1/n_f \mathcal{E}(k; n_f, T_f)]. \quad (\text{A1})$$

In this equation,  $D^0$  is the short-time self-diffusion coefficient, related by Einstein's relation with the corresponding short-time friction coefficient  $\zeta^0 = k_B T / D^0$  which, for colloidal liquids, can be determined by its Stokes expression. The function  $\mathcal{E}(k; n_f, T_f)$ , on the other hand, is the Fourier transform (FT) of the functional derivative  $\mathcal{E}[|\mathbf{r} - \mathbf{r}'|; n, T] \equiv [\delta\beta\mu[\mathbf{r}; n] / \delta n(\mathbf{r}')]$  of the chemical potential  $\mu[\mathbf{r}; n]$  with respect to the local concentration profile  $n(\mathbf{r})$ , evaluated at the uniform concentration and temperature profiles  $n(\mathbf{r}) = n_f$  and  $T(\mathbf{r}) = T_f$  of the final state. This property is a fundamental thermodynamic input of the theory, whose practical determination is discussed below.

The time-evolving mobility function  $b(t)$  appearing in the right side of Eq. (A1) is defined as  $b(t) \equiv D_L(t) / D^0$ , with  $D_L(t)$  being the long-time self-diffusion coefficient of the colloidal particles at evolution time  $t$ . As explained in Refs. [47, 49], the equation

$$b(t) = [1 + \int_0^\infty d\tau \Delta\zeta^*(\tau; t)]^{-1} \quad (\text{A2})$$

relates  $b(t)$  with the  $t$ -evolving and  $\tau$ -dependent friction coefficient  $\Delta\zeta^*(\tau; t)$ , given approximately by

$$\Delta\zeta^*(\tau; t) = \frac{D_0}{24\pi^3 n_f} \int d\mathbf{k} k^2 \left[ \frac{S(k; t) - 1}{S(k; t)} \right]^2 F(k, \tau; t) F_S(k, \tau; t). \quad (\text{A3})$$

Thus, the presence of  $b(t)$  in Eq. (A1) couples  $S(k; t)$  with the non-stationary two-time density correlation functions  $F(k, \tau; t) \equiv \langle \sum_{n, n'}^N \exp(i\mathbf{k} \cdot [\mathbf{r}_n(t + \tau) - \mathbf{r}_{n'}(t)]) \rangle$  and  $F_S(k, \tau; t) = \langle \exp[i\mathbf{k} \cdot \Delta\mathbf{r}_T(\tau, t)] \rangle$ , for which the NE-SCGLE also provides time evolution equations. In terms of their Laplace transforms (LT)  $F(k, z; t)$  and  $F_S(k, z; t)$ , such equations read,

$$F(k, z; t) = \frac{S(k; t)}{z + \frac{k^2 D^0 S^{-1}(k; t)}{1 + \lambda(k) \Delta\zeta^*(z; t)}}, \quad (\text{A4})$$

and

$$F_S(k, z; t) = \frac{1}{z + \frac{k^2 D^0}{1 + \lambda(k) \Delta\zeta^*(z; t)}}, \quad (\text{A5})$$

with  $\lambda(k)$  being a phenomenological interpolating function [50], given by

$$\lambda(k) = 1/[1 + (k/k_c)^2], \quad (\text{A6})$$

with  $k_c$  being an empirically-chosen cutoff wave-vector. This parameter can be employed to calibrate the theory in each specific application, as indicated in Section III.

The solution of Eqs. (A1)-(A5) provides the t-evolution of the functions  $S(k; t)$ ,  $b(t)$ ,  $\Delta\zeta^*(t)$ ,  $F(k, \tau; t)$  and  $F_S(k, \tau; t)$ , which describe the irreversible relaxation of an instantaneously and homogeneously quenched liquid. Specific details regarding the numerical solution of Eqs. (A1)-(A5) can be found in Ref. [49] and access to a computational code to solve these equations is provided in [55].

## Appendix B: Simulation details

Our Brownian dynamics simulations of  $N$  particles interacting through the soft repulsive potential in Eq. (2.1), were conducted in a cubic simulation box of volume  $V$  with periodic

boundary conditions. The positions of the particles in the simulation cell were updated according to the conventional Ermak-McCammon algorithm [75]

$$\mathbf{r}(t + \Delta t) = \mathbf{r}(t) + \beta D^0 \mathbf{F}(t) + \delta \mathbf{R}, \quad (\text{B1})$$

where  $\Delta t$  is the time step,  $\mathbf{r}(t)$  and  $\mathbf{F}(t)$  the position and force on the particle at time  $t$ , and  $\delta \mathbf{R}$  represents, for each Cartesian component, a random displacement extracted from a Gaussian distribution with zero mean and variance  $2D^0 \Delta t$ . Our simulations followed the quench protocol introduced in this work. The samples were prepared and lead to equilibrium at the temperature  $T_i$ , and then quenched to the target temperature  $T_f$  using  $N = 10000$  particles. This stage of the simulations was conducted for at least  $500t_B$  (where  $t_B = \sigma^2/D^0$  is the Brownian time), using a step time  $\Delta t = 10^{-4}t_B$  for most of the systems; for some systems  $\Delta t = 5 \times 10^{-5}t_B$  was used. To simulate polydisperse systems we introduced a size polydispersity  $P$  by taking the diameters of the  $N$  particles evenly distributed between  $\bar{\sigma}(1 - w/2)$  and  $\bar{\sigma}(1 + w/2)$ , with  $\bar{\sigma}$  the mean diameter of the distribution and for the particular value of  $P = 0.1$ . Further details of our simulations can be found in Refs. [50] and [74].

- 
- [1] L. Cipelletti and L. Ramos, *J. Phys.: Condens. Matter* **17**(2005) R253-R285.
  - [2] P. Lunkenheimer, R. Wehn, U. Schneider, and A. Loidl, *Phys. Rev. Lett.*, **95** 055702 (2002)
  - [3] T. Hecksher, N.B. Olsenb, K. Nissc, and J.C. Dyre *J. Chem. Phys.*, **133** 174514 (2010).
  - [4] L. Cipelletti, L. Ramos, s. Manley, E. Pitard, D. A. Weitz, E.E. Pashkovski, and M. Johansson, *Faraday Discuss.* **123**, 237 (2003).
  - [5] X. Di, K. Z. Win, G. B. McKenna, T. Narita, F. Lequeux, S. R. Pullela, and Z. Cheng, *Phys. Rev. Lett.* **106**, 095701 (2011)
  - [6] R. Bandyopadhyay, D. Liang, H. Yardimci, D.A. Sessoms, M.A. Borthwick, S.G.J. Mochrie, J.L. Harden, and R.L. Leheny, *Phys. Rev. Lett.* **93**, 228302
  - [7] H. Bissig, S. Romer, L. Cipelletti, V. Trappe, and P. Schurtenberger, *Phys. Chem. Commun.* **6**, 21 (2003).
  - [8] J. M.Hutchinson, *Progress in Polymer Science* Volume 20, Issue 4, 1995, 703-760.

- [9] L. Bellon, S. Ciliberto and C. Laroche, 2000 *Europhys Lett.*, **51**, 551.
- [10] A. Das, P.M. Derlet, C. Liu, E.M. Dufresne and Robert Maaß, *Nat. Commun.* **10**, 5006 (2019).  
<https://doi.org/10.1038/s41467-019-12892-1>.
- [11] B. Ruta, G. Baldi, G. Monaco and Y. Chushkin *J. Chem. Phys.* **138**, 054508 (2012).
- [12] A. Knaebel, M. Bellour, J. P. Munch, V. Viasnoff, F. Lequeux, and J. L. Harden, *Europhys. Lett.* **52**, 73 (2000).
- [13] B. Ruzicka, E. Zaccarelli, L. Zulian, R. Angelini, M. Sztucki, A. Moussaid, T. Naryanan and F. Sciortino, *Nature Materials* **10**, 56–60 (2011).
- [14] R. Angelini *et al.* *Nat. Commun.* **5**:4049 doi: 10.1038/ncomms5049 (2014).
- [15] L. Cipelletti, S. Manley, R. C. Ball, and D. A. Weitz, *Phys.Rev. Lett* **84**, 2275 (2000).
- [16] A. Jain, F. Schulz, I. Lokteva, L. Frenzel, G. Grübel and F. Lehmkuhler, *Soft Matter* 2020, **16**, 2864-2872.
- [17] M.M Gordon, *Journal of Rheology* **61**, 23 (2017).
- [18] A. R. Jacob, E. Moghimi, and G. Petekidis, *Physics of Fluids* **31**, 087103 (2019).
- [19] D. Bonn, H. Tanaka, G. Wegdam, H. Kellay and J. Meunier *Europhys Lett.* **45**(1), pp.52-57 (1999)
- [20] B. Abou, D. Bonn, and J. Meunier, *Phys. Rev. E* **64**, 021510 (2001).
- [21] D. El Masri, M. Pierno, L. Berthier and L. Cipelletti, *J. Phys.: Condens. Matter* **17** S3543, (2005).
- [22] V. A. Martinez, G. Bryant, and W. van Meegen, *Phys. Rev. Lett.* **101**, 135702 (2008).
- [23] E. Sanz *et al.*, *J. Phys. Chem. B* **112**, 10861 (2008).
- [24] P. J. Lu *et al.*, *Nature* **453**: 499 (2008).
- [25] W. Kob and J.-L. Barrat, *Phys. Rev. Lett.* **78**, 4581 (1997).
- [26] G. Foffi, E. Zaccarelli, S. Buldyrev, F. Sciortino, and P. Tartaglia, *J. Chem. Phys.* **120**, 8824 (2004).
- [27] A. M. Puertas, *J. Phys.: Condens. Matter* **22**, 104121 (2010).
- [28] M. Warren and J. Rottler, *Phys. Rev. Lett.*, **110**, 025501 (2013).
- [29] P. De Gregorio *et al.*, *Physica A*, **307**, 15 (2002).
- [30] L. F. Cugliandolo and J. Kurchan, *Phys. Rev. Lett.* **71**, 173 (1993).
- [31] A. Latz, *J. Phys. Condens. Matter* **12**, 6353-6363 (2000).
- [32] A. Latz, *J Stat. Phys.*, **109**, 607 (2002).



- [33] B. Kim and A. Latz, *Europhys Lett.* **53**, 660 (2001).
- [34] W. Götze, in *Liquids, Freezing and Glass Transition*, edited by J. P. Hansen, D. Levesque, and J. Zinn-Justin (North-Holland, Amsterdam, 1991).
- [35] W. Götze and L. Sjögren, *Rep. Prog. Phys.* **55**, 241 (1992).
- [36] W. Götze and E. Leutheusser, *Phys. Rev. A* **11**, 2173 (1975).
- [37] W. Götze, E. Leutheusser and S. Yip, *Phys. Rev. A* **23**, 2634 (1981).
- [38] L. Yeomans-Reyna and M. Medina-Noyola, *Phys. Rev. E* **64**, 066114 (2001).
- [39] L. Yeomans-Reyna, H. Acuña-Campa, F. Guevara-Rodríguez, and M. Medina-Noyola, *Phys. Rev. E* **67**, 021108 (2003).
- [40] R. Juárez-Maldonado *et al.*, *Phys. Rev. E* **76**, 062502 (2007).
- [41] M. A. Chávez-Rojo and M. Medina-Noyola, *Physica A* **366**, 55 (2006).
- [42] M. A. Chávez-Rojo and M. Medina-Noyola, *Phys. Rev. E* **72**, 031107 (2005); *ibid* **76**: 039902 (2007).
- [43] L. Yeomans-Reyna, M. A. Chávez-Rojo, P. E. Ramírez-González, R. Juárez-Maldonado, M. Chávez-Páez, and M. Medina-Noyola, *Phys. Rev. E* **76**, 041504 (2007)
- [44] R. Juárez-Maldonado and M. Medina-Noyola, *Phys. Rev. E* **77**, 051503 (2008).
- [45] L. E. Sánchez-Díaz, A. Vizcarra-Rendón, and R. Juárez-Maldonado, *Phys. Rev. Lett.* **103**, 035701 (2009).
- [46] L.F. Elizondo-Aguilera and Th. Voigtmann, *Phys. Rev. E* **100** 042601, (2019).
- [47] P. E. Ramírez-González and M. Medina-Noyola, *Phys. Rev. E* **82**, 061503 (2010).
- [48] P. E. Ramírez-González and M. Medina-Noyola, *Phys. Rev. E* **82**, 061504 (2010).
- [49] L. E. Sánchez-Díaz, P. E. Ramírez-González and M. Medina-Noyola, *Phys. Rev. E* **87**, 052306 (2013).
- [50] G. Perez, et al. *Phys. Rev. E* **83**, 060501(R) (2011).
- [51] P. Mendoza-Méndez, E. Lázaro-Lázaro, L. E. Sánchez-Díaz, , P. E. Ramírez-González, G. Pérez-Ángel, and M. Medina-Noyola, *Physical Review E* **96**, 022608 (2017)
- [52] J.M. Olais-Govea, L. López-Flores, and M. Medina-Noyola, *J. Chem Phys.* **143**, 174505 (2015).
- [53] J.M. Olais-Govea, L. López-Flores, and M. Medina-Noyola, *Phys. Rev. E* **98**, 040601(R) (2018).
- [54] J.M. Olais-Govea, B. Zepeda-López, L- López-Flores, and M. Medina-Noyola, *Scientific Reports* **9**, 16445 (2015).

- [55] J.B. Zepeda-López and M. Medina-Noyola *J. Chem. Phys.* **154**, 174901 (2021)
- [56] G. Brambilla, D. El Masri, M. Pierno, L. Berthier, L. Cipelletti, G. Petekidis, and A. B. Schofield, *Phys. Rev. Lett.* **102**, 085703 (2009)
- [57] D. El Masri, G. Brambilla, M Pierno, G. Petekidis, A. B. Schofield, L. Berthier and L. Cipelletti, *Journal of Statistical Mechanics Theory and Experiment* **2009**, P07015 (2009)
- [58] D. A. Sessoms, I. Bischofberger, L. Cipelletti, and V. Trappe, *Phil. Trans. R.Soc. A* **367**, 5013 (2009).
- [59] R. Rivas-Barbosa, E. Lázaro-Lázaro, P. Mendoza-Méndez, T. Still, V. Piazza, P.E. Ramírez-González, M. Medina-Noyola and M. Laurati
- [60] H.C. Andersen, J.D. Weeks and D. Chandler, *Phys. Rev. A* **4**, 1597 (1971).
- [61] P. Mendoza-Méndez, L. López-Flores, A. Vizcarra-Rendón, L. E. Sánchez-Díaz, and M. Medina-Noyola, *Physica A (Amsterdam)* **394**, 1 (2014).
- [62] G. E. Uhlenbeck and L. S. Ornstein, *Phys. Rev.* **36**, 823 (1930).
- [63] J. K. Percus and G. J. Yevick, *Phys. Rev.* **110**, 1 (1957).
- [64] L. Verlet and J.-J. Weis, *Phys. Rev. A* **5**, 939 (1972).
- [65] J. P. Hansen and I.R. McDonald, *Theory of Simple Liquids* (Academic Press, San Diego, 1976).
- [66] P. G. de Gennes, *Physica* **25**, 825 (1959).
- [67] K. Kim and S. Saito, *Phys. Rev. E* **79**, 060501(R) (2009).
- [68] E.C. Cortés Morales, L.F. Elizondo-Aguilera and M. Medina-Noyola, *J. Phys. Chem. B* 2016, **120** 7975-7987.
- [69] R. Peredo-Ortiz, P.F. Zubieta-Rico, E.C. Cortés-Morales, G. Pérez-Ángel, Th. Voigtmann, M. Medina-Noyola and L.F. Elizondo-Aguilera, *J. Phys.: Condens. Matter* **34** (2022) 084003.
- [70] P.E. Ramírez-González, L. López-Flores, H. Acuña Campa and M. Medina-Noyola, *Phys. Rev. Lett.*, **107**, 155701 (2011).
- [71] T. Rizzo and Th. Voigtmann, *Europhys. Letters* **111**, 56008 (2015).
- [72] T. Rizzo and Th. Voigtmann, *Phys. Rev. Lett.* **124**, 195501 (2020).
- [73] L.F. Elizondo-Aguilera, T. Rizzo and Th. Voigtmann arXiv:2202.13384 [cond-mat.soft] (2022).
- [74] L. López-Flores, H. Ruiz-Estrada, M. Chávez-Páez, and M. Medina-Noyola, *Phys. Rev. E* **88**, 042301 (2013).
- [75] M.P. Allen y D.J. Tildesley, *Computer Simulation of Liquids*, Clarendon Press, Oxford, 1987.